Final Report

ONR Grant N00014-93-1-0053

1 November 1993 — 30 June 1997

Energetic Fuel Droplet Gasification with Liquid-Phase Reaction

Prepared by William A. Sirignano and David N. Schiller

Department of Mechanical and Aerospace Engineering
University of California, Irvine 92697

DISTRIBUTION STATEMENT A
Approved for public release;
Distribution Unlimited

Submitted to Dr. Gabriel Roy, Scientific Officer

15 May 1998

DTIC QUALITY INSPECTED 1

19980603 092

Abstract

An analytical and computational study of the gasification and oxidation of an energetic liquid fuel droplet is presented. Single-step, finite-rate, Arrhenius reaction rate expressions are used for exothermic liquid-phase decomposition and gas-phase oxidation. The liquid fuel is assumed to decompose to a gaseous product at a fixed number of bubble sites per unit mass (specified *a priori*) within the droplet. Decomposed gas escapes the droplet surface by: (1) decomposition (gasification) of the droplet surface, (2) decomposition at the surface of bubbles that connect with the droplet surface, and (3) escape of gas inside bubbles due to droplet surface regression. Without oxidation, results are compared between one model wherein gaseous fuel leaves the droplet due to decomposition of the droplet surface and bubbles that connect with the droplet surface when the void fraction exceeds a critical value (ϕ_c), and another model wherein the droplet mass decreases due to discontinuous bubble bursting at the droplet surface. The models agree well (with the exception of oscillations in the droplet radius predicted by the latter model) in the limit of $\phi_c \to 1$.

The transient, two-phase, governing equations are solved numerically for various values of the nondimensional reaction rate coefficients (for both decomposition and oxidation), heats of decomposition and oxidation, number of bubbles per unit mass (N/m), and ambient temperature and pressure. Consistent with simplified scaling for the limit of chemical rate control, the droplet lifetime $\eta_{d,*}$ is strongly dependent on the nondimensional decomposition rate constant and activation energy, and less strongly on the number of bubbles per unit mass, ambient pressure, and heat of decomposition. Increasing the ratio of gas-phase to liquid-phase thermal conductivities increases $\eta_{d,*}$ slightly. The droplet lifetime is a monotonically increasing function of initial droplet radius but too weak for diffusion rate control: the results are closer to the chemical rate control limit.

After an ignition delay period, the flame radius is predicted to increase nearly linearly with time until the droplet is gasified. After this time ($\eta_{d,*}$), the flame radius decreases with time. The variation of flame radius with time differs from classical droplet burning due to the exothermic decomposition process that determines the gasification rate. Simplified scaling previously derived for the droplet lifetime also correlates the effect of decomposition parameters on the flame behavior.

Gas-phase oxidation does not appreciably affect the droplet lifetime, for the selected base case values of the above parameters, because droplet heating is controlled primarily by the liquid-phase decomposition. As the decomposition rate is reduced (e.g., by reducing N/m), the time scale for heat conduction from the flame to the droplet becomes comparable to that of liquid decomposition, and hence gas-phase oxidation significantly reduces $\eta_{d,*}$. For the base case, liquid-phase decomposition increases the flame temperature by approximately 6%. Therefore, energetic liquid fuels can be expected to vaporize and burn more rapidly and to yield more thermal energy than conventional hydrocarbon fuels.

NOMENCLATURE

A_{lg} surface area of liquid/gas interface per unit mass of fluid
C_p specific heat

E_c activation energy for gas-phase oxidation
E_d activation energy for liquid-phase decomposition
G gasification rate per unit surface area of liquid/gas interface
k_c rate constant for gas-phase oxidation
k_d rate constant for liquid-phase decomposition
Le_g Lewis number, $\lambda'/(\rho_{g,*}C_p'\mathcal{D}_*)$
p ambient pressure
Q_c heat release rate per unit mass of fuel due to gas-phase oxidation
Q_d heat release rate per unit mass of fuel due to liquid-phase decomposition
R_b gas pocket (bubble) equivalent radius
r nondimensional radius, r'/r_o'
r_o' initial droplet radius
$\mathcal{R}_u$ universal gas constant
t time
T temperature
v_r radial velocity
Y_i mass fraction of species i

Greek Symbols

β weighting factor for the reduction of bubble surface area due to bubble connecting
η nondimensional time, $\eta'\mathcal{D}_*/r_o'^2$
$\eta_{c,*}$ time at which 99% of the initial droplet mass has oxidized in the gas phase
$\eta_{d,*}$ time at which 99% of the initial droplet mass has gasified (droplet lifetime)
$\omega_{c,i}$ species consumption rate due to gas-phase oxidation
ω_d gasification (decomposition) rate per unit volume of fluid
ϕ void (gas volume) fraction
ϕ_c critical packing value; bubbles connect when $\phi \geq \phi_c$
ψ mass coordinate divided by 4π
$\rho_{g,*}$ gas-phase reference density (air at P_∞', T_∞')
ρ material gas density
ρ_l material liquid density
$\overline{\rho}$ bulk gas density
$\overline{\rho}_l$ bulk liquid density
τ time in von Mises plane
θ nondimensional temperature, $(T' - T_o')/(T_\infty' - T_o')$, where $T_o' = 300$ K
ξ normalized mass coordinate, ψ/ψ_s

Subscripts

$*$ reference property evaluated at 300 K for the liquid phase and at T_∞' for the gas phase
fl flame (point of maximum fuel consumption rate)
g gas phase; subscript sometimes omitted
i gas-phase species (e.g., F, fuel vapor; P, products)
l liquid phase
s droplet surface

Other nomenclature is defined when first used in the text. Dimensional variables are denoted with a prime ($'$) and nondimensional variables are unprimed.

INTRODUCTION

The additional flight range available with high-energy, strained-molecule fuels such as benzvalene is highly attractive. The relative chemical instability associated with the new fuels introduces new physics and chemistry into the droplet vaporization problem. The exploration of this new science is important and challenging from both the practical and the intellectual points of view. The most critical new feature is the occurrence of exothermic reactions in the liquid phase. Upon heating, some of the chemical bonding in the liquid fuel will be broken, releasing more energy and yielding simpler hydrocarbons. Thermodynamic analysis indicates that the decomposition energy per unit mass of a strained hydrocarbon fuel is one order of magnitude less than the energy per unit mass of fuel released in oxidation. In oxidation, however, the energy is shared with a mass one order of magnitude larger than the mass of fuel due to mixing of the fuel with air. Adiabatic temperatures for oxidation of conventional fuels and for decomposition of strained fuels are therefore of the same order of magnitude. For example, according to Moriarty and Rao (1993), benzvalene has a strain energy of 4.13×10^6 J/kg. Published heats of combustion and vaporization for benzene are 4.06×10^7 J/kg and 3.95×10^5 J/kg, respectively.

Law and co-workers (Lee *et al.*, 1988, 1989 and 1992) conducted experimental studies of the vaporization, combustion, microexplosion, and thermophysical and thermochemical properties of organic azides. They found that the quiescent gasification rate of droplets of organic azides is greater than the corresponding hydrocarbons, and they attributed this to liquid-phase decomposition either within the droplet or at the droplet surface (Lee *et al.*, 1988). While monoazides were found to closely fit a Clausius-Clapeyron relation over a broad temperature range, diazides heavier than diazidohexane did not follow such a relation. It was hypothesized that decomposition both in the liquid phase as well as upon gasification can occur in the heavy diazides. This hypothesis was later supported by droplet experiments performed at elevated pressures (Lee *et al.*, 1992). As the pressure was increased in these experiments, a large gasification rate increase was observed for diazides but not for monoazides or hydrocarbons of equal volatility. Liquid-phase reactions were found to increase due to dihalide addition and droplet temperature elevation. By using the burning rate constant in the classical d^2-Law expression to interpret their experimental results, Lee *et al.* (1989) conjectured that decomposition occurs in the droplet interior and/or at the droplet surface rather than in the surrounding gas phase. Lee *et al.* (1989), however, did not observe evidence of liquid decomposition in monoazide droplets heated up to 500 K. Microexplosions were observed in organic azide droplets (Lee *et al.*, 1988), which is a strong indicator of bubble formation. It is possible that (1) the bubbles were too small to detect, and/or (2) the microexplosion of the droplets was caused by bubbles formed so rapidly that they were not detected.

It is interesting to note that liquid-phase reactions might also occur in the combustion of high-energy solid fuels such as HMX and boron/poly(BAMO/NMMO) fuel-rich solid propellants. Palopoli and Brill (1991) describe subsurface reactions that create a heterogeneous "foam zone" in the condensed phase of HMX. A subsurface reaction zone was also

described by Hsieh *et al.* (1991) for the combustion of boron/poly(BAMO/NMMO). The liquid layer that is observed during the rapid thermal decomposition of HMX is formed by condensed-phase liquefaction with concomitant decomposition rather than true melting (Brill and Karpowicz, 1982; Palopoli and Brill, 1991).

Experiments have not yet revealed useful information on the rates of fuel decomposition, liquid vaporization, and gas-phase mixing. In particular, droplet experiments have only been performed with the high-energy fuels strongly diluted by conventional fuels (Law, 1995). Theoretical and numerical analyses should reveal vital information about the reaction zone in the liquid where reactants and gaseous products exist together.

The high energy fuel can conceivably decompose in at least three ways: (1) high temperatures might cause the strained fuel to vaporize and then decompose and burn in the gas phase; (2) the liquid decomposes to a liquid product that gasifies: and (3) the liquid decomposes to a gaseous product. The first path requires a greater stability for the strained fuel in order for the fuel to vaporize without decomposing. The heavier molecule of the original strained fuel would be short-lived under gas-phase collisions. The very large heat release due to decomposition would probably make the lifetime of the product as a liquid negligible, thus making path (2) unlikely. This leaves the third path as a likely case and the one that is studied herein.

The third path requires a very hot liquid vaporizing in depth. On the fine scale, gasification has a distribution of nucleation sites throughout the hot liquid interior. At the high temperatures, nucleation is occurring faster than outer droplet surface regression so that bubbles should result. The liquid is being heated so rapidly that the outer surface cannot accommodate vaporization quickly enough to maintain phase equilibrium. As the liquid superheats, other nucleation sites in the liquid interior are given time to develop.

The liquid-phase reaction is most likely to occur in the warmer portion of the droplet near the surface rather than the cooler domain in the center of the droplet. The exothermic liquid-phase reaction will augment the heating of the reactants (strained fuel) and the products (still a hydrocarbon fuel) in this reacting domain. Existing droplet vaporization analyses do not treat the change of phase within the droplet interior that can result from this heat release. It is not reasonable to expect the liquid-phase reaction to occur in a very thin spherical shell around the edge of the droplet; this would require very fast reactions at the relatively low liquid temperatures. More likely, the reaction occurs over a finite domain where both liquid and gas exist. With large enough gaseous content, all of the gas cannot remain in solution, but rather bubbles should form. It is reasonable to expect, therefore, that a bubbly region will exist near the surface that consists of liquid fuel reactant and gaseous fuel products. This two-phase bubbly region exists between the pure liquid and the surrounding gas.

Figures 1 and 2 show schematics of the vaporizing liquid-fuel energetic droplet with and without gas-phase oxidation. The model both temporally and spatially resolves all three regions of the problem: the surrounding gas film, two-phase bubbly layer, and the liquid droplet core. The decomposed energetic liquid fuel forms bubbles in the droplet, causing the droplet to swell before the droplet radius decreases due to the transport of decomposed liquid to the surrounding gas film. Fuel vapor is assumed to cross the interface of the droplet and enter the gas phase (i.e., gasify) by three mechanisms: (1) decomposition (gasification) of the droplet surface, (2) decomposition at the surface of bubbles in the droplet that connect with the droplet surface either by intersecting the droplet surface or by connecting with

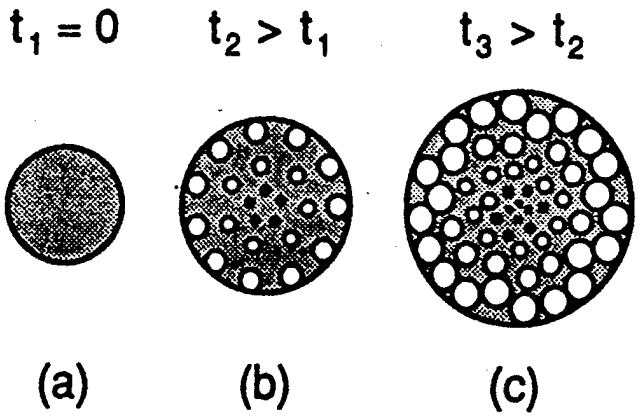

Figure 1: Schematic of the vaporizing liquid-fuel energetic droplet without gas-phase oxidation: (a) shows the initial droplet ($t_1 = 0$), while (b) and (c) show the droplet at progressively larger times, t_2 and t_3.

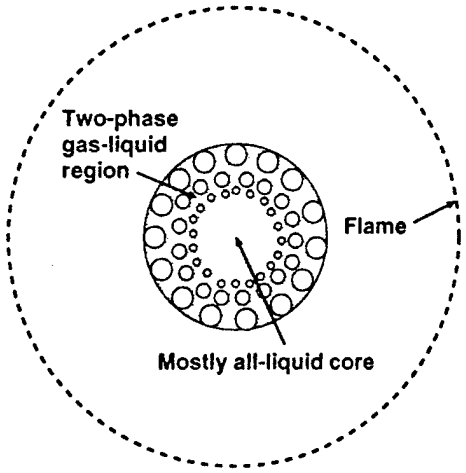

Figure 2: Schematic of the vaporizing liquid-fuel energetic droplet with gas-phase oxidation.

other bubbles that intersect the droplet surface, and (3) escape of gas inside a bubble due to droplet surface regression. Results using this decomposition model are compared below to an alternative model that assumes that the droplet mass decreases due to discontinuous bubble bursting at the droplet surface. Unless otherwise specified, bubbles are assumed to connect with the droplet surface (mechanism #2 above) when the void fraction exceeds a critical packing value, $\phi_c = 0.8$.

The model's input parameters include initial droplet temperature, ambient pressure and temperature, gas and liquid densities, specific heat, Lewis number, and the following nondimensional parameters: rate constants (for both the decomposition rate and oxidation rate expressions), heats of decomposition and oxidation, number of bubbles per unit mass, and ratio of gas-phase to liquid-phase thermal conductivities. A parametric study is performed below on some of these key parameters to determine the effects of gas-phase oxidation on the droplet lifetime, as well as the effects of the liquid-phase decomposition on the flame radius, flame temperature, and gas-phase profiles of temperature and species mass fractions.

ANALYSIS

The continuity, energy, and species conservation equations are solved numerically using a von Mises formulation with a mass coordinate that is normalized by the droplet mass. Gas-phase oxidation and liquid-phase decomposition are modelled by exothermic, single-step, finite-rate Arrhenius chemical reaction rate expressions. In the simplified model used here, mass diffusion in the liquid phase is not considered. Therefore, the gas bubbles in the liquid droplet contain only decomposed fuel vapor that does not dissolve back into the liquid phase. The following additional assumptions are made: (1) mass diffusion in the liquid phase, transport of heat by mass diffusion, kinetic energy, and viscous dissipation are neglected; (2) the momentum equation is replaced by assuming zero pressure gradients; (3) spherically-symmetric geometry, (4) bubbles are spherical and do not migrate; (5) the specific heats of the vapor and the liquid are assumed equal and constant (a reasonable assumption for higher molecular weight hydrocarbons); (6) the decomposed gas is assumed to be benzene ($M_F = 78.11$); (7) droplet shattering, microexplosions and the breakup of bubbles are neglected (the number of bubbles per unit mass is assumed constant); (8) the change in gas/liquid interface area due to the coalescence of bubbles is neglected; and (9) the material density of the liquid is constant, $\rho_l' = 1000$ kg/m^3. This value of liquid density is representative of many energetic liquid fuels that commonly exist in liquid form. Varying ρ_l' from 700 to 1300 kg/m^3 does not change qualitatively the results of this study. For comparison, Law and co-workers (Law, 1996) have studied liquid dihydrobenzvalene ($\rho_l' = 854$ kg/m^3) and liquid methylcubane ($\rho_l' = 1010$ kg/m^3).

The key assumptions of the model are: (1) the use of single-step reaction rate expressions for decomposition and gas-phase oxidation, and (2) the *a priori* specification of bubble site locations. Our objective is to study qualitatively the effects of various fundamental nondimensional groupings on the gasification and oxidation of an energetic liquid fuel. The use of one-step decomposition kinetics clearly oversimplifies the complicated chemistry involved in the problem but is both practical and necessary without additional information about the individual decomposition reaction steps. Gas-phase oxidation is expected to occur relatively fast, so the use of a one-step finite-rate reaction expression is arguably a sufficient

improvement to an assumption of infinite-rate reactions. The present model assumes there are a specified number of bubble sites per unit mass (N/m) rather than relying on kinetic theory to predict the location of bubble sites. In practice, it is possible that the number of bubbles might be controlled through seeding with tiny particles and the encouragement of heterogeneous nucleation.

Let o denote the void mass fraction in a two-phase gas-liquid region. Then, $0 < o < 1$: ϕ=1 in the gas phase; and ϕ=0 in the liquid phase. The bulk density for the gas is $\overline{\rho}' = o\rho'$, and for the liquid it is $\overline{\rho}'_l = (1-\phi)\rho'_l$. Under the assumptions above, the transient, dimensional conservation equations are as follows:

Conservation of mass:

$$\frac{\partial(\overline{\rho}' + \overline{\rho}'_l)}{\partial t'} + \frac{1}{r'^2}\frac{\partial}{\partial r'}\left[r'^2(\overline{\rho}' + \overline{\rho}'_l)v'_r\right] = 0 \tag{1}$$

Conservation of energy:

$$(\overline{\rho}' + \overline{\rho}'_l)\left(\frac{\partial T'}{\partial t'} + v'_r\frac{\partial T'}{\partial r'}\right) = \frac{p'}{C'_p}\frac{\partial \phi}{\partial t'} + \dot{w}'_d\frac{Q'_d}{C'_p} + \omega'_{c,F}\frac{Q'_c}{C'_p} + \frac{1}{C'_p r'^2}\frac{\partial}{\partial r'}\left(r'^2\lambda'_{2,\phi}\frac{\partial T'}{\partial r'}\right) \tag{2}$$

Conservation of species mass in the gas phase surrounding the droplet (where $\phi = 1$):

$$\rho'\left(\frac{\partial Y_i}{\partial t'} + v'_r\frac{\partial Y_i}{\partial r'}\right) = \frac{1}{r'^2}\frac{\partial}{\partial r'}\left(r'^2\rho'\mathcal{D}_*\frac{\partial Y_i}{\partial r'}\right) - \omega'_{c,i} \tag{3}$$

Here $\omega'_{c,i}$ is the consumption rate of species i due to gas-phase oxidation.

The property variations (in space and time) result from varying temperature and composition of the two-phase zone. Several studies are available to predict thermal conductivity of a mixture. Here, we use the general mixture rule from Nielsen (1978) with the reduced concentration term equal to unity:

$$\frac{\lambda'_{2,\phi}}{\lambda'_l} = \frac{1 + ABo}{1 - Bo} \tag{4}$$

where A is a constant that depends on the shape of the bubbles, state of agglomeration, and nature of the interface. We assume spherical bubbles in our case so that $A = 2$ (Nielsen, 1978). The constant B is given by

$$B = \frac{\lambda'/\lambda'_l - 1}{\lambda'/\lambda'_l + A} \tag{5}$$

Note that $\lambda'_{2,\phi} = \lambda'_l$ when $\phi = 0$ and $\lambda'_{2,\phi} = \lambda'_g$ when $o = 1$.

The equation of state is given by

$$\overline{\rho}' = \phi\rho' = \phi p' M/\mathcal{R}'_u T' \tag{6}$$

where M is the mean molecular weight of the mixture of air and decomposed gas.

The gasification rate (or liquid mass loss rate) per unit area of gas-liquid interface is assumed to be

$$G' = k'_d \exp(-E'_d/\mathcal{R}'_u T') \qquad [\mathrm{kg/m^2 \cdot s}] \tag{7}$$

The rate constant k'_d and the activation energy E'_d depend upon the type of the liquid fuel. The problem is closed for a particular value of k'_d and E'_d. If A'_{lg} denotes the total surface area of liquid/gas interface per unit mass of fluid, then the total gasification rate per unit volume of fluid is

$$\omega'_d = A'_{lg}(\overline{\rho}' + \overline{\rho}'_l)G' \qquad [\mathrm{kg/m^3 \cdot s}] \tag{8}$$

If R'_b denotes the equivalent average bubble radius, then $A'_{lg} = 4\pi R'^2_b(N'/m')$ in the interior of the droplet if the bubbles do not touch each other. As discussed below, different equations for A'_{lg} arise due to either gasification of the droplet surface or the reduction of bubble surface area due to bubble connecting.

The number of bubbles (bubble centers) per unit mass, N'/m', is related to the number of bubbles per unit volume (the bubble number density, n') by

$$\frac{N'}{m'} = \frac{n'}{\overline{\rho}' + \overline{\rho}'_l} = \text{constant} \tag{9}$$

The void fraction is

$$\phi = \frac{4\pi R'^3_b n'}{3} \tag{10}$$

Also, the rate of change of bubble radius is given by

$$\frac{dR'_b}{d\tau'} = \frac{G'}{\rho'_g} - \frac{R'_b}{3\rho'_g}\frac{d\rho'_g}{d\tau'} \tag{11}$$

where ρ'_g is the density of the gaseous products from the decomposition of the liquid. Eq. (11) is derived from a Lagrangian analysis (see von Mises transformation below).

The fuel consumption rate due to gas-phase oxidation is

$$\omega'_{c,F} = k'_c \rho'^2 Y_F Y_{O_2} \exp(-E'_c/\mathcal{R}'_u T') \tag{12}$$

Assuming a stoichiometric reaction of benzene, $\omega'_{c,O_2} = 3.077\omega'_{c,F}$ and $\omega'_{c,P} = -4.077\omega'_{c,F}$. For the present study, values of $k'_c = 3.6 \times 10^9$ m^3/kg·s and $E'_c = 30$ kcal/mole were selected from hydrocarbon fuel data (Westbrook and Dryer, 1981), and $Q'_c = 4.06 \times 10^7$ J/kg is that of benzene.

Nondimensional Equations After Coordinate Transformations

When the droplet swells due to bubble formation, the droplet radius changes whereas the droplet mass remains fixed if gasification of the droplet surface were negligible. Therefore, a von Mises transformation (Chervinsky, 1969; Bhatia and Sirignano, 1992) is applied so that coordinates are changed from an Eulerian time and radius (t', r') to a Lagrangian time and mass coordinate (τ', ψ'), where $\tau' = t'$,

$$\frac{\partial}{\partial \tau'} = \frac{\partial}{\partial t'} + v'_r \frac{\partial}{\partial r'} \tag{13}$$

and the stream function ψ' is defined as

$$\frac{\partial \psi'}{\partial t'} = -r'^2(\overline{\rho}' + \overline{\rho}'_l)v'_r \quad , \quad \frac{\partial \psi'}{\partial r'} = r'^2(\overline{\rho}' + \overline{\rho}'_l) \tag{14}$$

Note that Eq. (14) satisfies Eq. (1).

In order to provide a fixed boundary with respect to the regressing droplet, a final coordinate transformation is made from (τ', ψ') to (η', ξ) where

$$\xi = \psi'/\psi'_s \ , \ \eta' = \tau' \ , \ \frac{\partial}{\partial \tau'} = \frac{\partial}{\partial \eta'} - \xi \frac{\dot{\psi}'_s}{\psi'_s} \frac{\partial}{\partial \xi} \tag{15}$$

Here ψ'_s and $\dot{\psi}'_s$ are the droplet mass and time derivative of the droplet mass (both divided by 4π), respectively. The evaluation of $\dot{\psi}'_s$ is discussed below. Note that ξ is nondimensional.

The radius of any given point is determined by:

$$r'^3 = 3\psi'_s \int_0^{\xi} \frac{d\hat{\xi}}{\overline{\rho}' + \overline{\rho}'_l} \tag{16}$$

where $\hat{\xi}$ is a dummy variable.

The nondimensional variables are defined as follows:

$$n = n' r'^3_o, \quad m = \frac{m'}{\rho'_l r'^3_o}, \quad r = \frac{r'}{r'_o}, \quad R_b = \frac{R'_b}{r'_o}, \quad \eta = \frac{\eta'}{r'^2_o/\mathcal{D}'}, \quad \psi = \frac{3\psi'}{\rho'_l r'^3_o}.$$

$$\overline{\rho} = \frac{\overline{\rho}'}{\rho'_l}, \quad \overline{\rho}_l = \frac{\overline{\rho}'_l}{\rho'_l} = 1 - \phi, \quad \rho_g = \frac{\rho'_g}{\rho'_l}, ; \quad v_r = \frac{v'_r}{\mathcal{D}'/r'_o}, \quad p = \frac{p'}{\rho'_l C'_p (T'_\infty - T'_o)}.$$

$$\theta = \frac{T' - T'_o}{T'_\infty - T'_o}, \quad Le_g = \frac{\lambda'}{\rho'_{g,*} C'_p \mathcal{D}_*}, \quad k_d = \frac{k'_d r'_o}{\rho'_l \mathcal{D}_*}, \quad Q_d = \frac{Q'_d}{C'_p (T'_\infty - T'_o)}$$

$$k_c = \frac{k'_d r'_o}{\rho'_l \mathcal{D}_*}, \quad Q_c = \frac{Q'_c}{C'_p (T'_\infty - T'_o)} \tag{17}$$

Other nondimensional groupings important to this problem include:

$$T'_\infty/T'_o, \quad N/m, \quad \lambda'/\lambda'_l, \quad \frac{E'_d}{\mathcal{R}'_u T'_o}, \quad \frac{E'_c}{\mathcal{R}'_u T'_o}$$

Using the above coordinate transformations and nondimensional variables, the mixture continuity, species and energy equations may be written as

$$-\frac{3r^2}{\psi_s}(\overline{\rho} + \overline{\rho}_l)^2 \frac{\partial v_r}{\partial \xi} - \frac{2}{r}(\overline{\rho} + \overline{\rho}_l) v_r = \frac{\partial (\overline{\rho} + \overline{\rho}_l)}{\partial \eta} - \xi \frac{\dot{\psi}_s}{\psi_s} \frac{\partial}{\partial \xi}(\overline{\rho} + \overline{\rho}_l) \tag{18}$$

$$\frac{\partial Y_i}{\partial \eta} - \xi \frac{\dot{\psi}_s}{\psi_s} \frac{\partial Y_F}{\partial \xi} = \frac{9\rho_{g,*}}{\psi_s^2} \frac{\partial}{\partial \xi} \left(r_g^4 \rho_g \frac{\partial Y_F}{\partial \xi} \right) - \frac{\omega_{c,i}}{\rho_g} \tag{19}$$

$$\frac{\partial\theta}{\partial\eta} - \xi\frac{\dot{\psi}_s}{\psi_s}\frac{\partial\theta}{\partial\xi} = \frac{9\rho_{g,*}}{\psi_s^2}Le_g\frac{\partial}{\partial\xi}\left[r^4\left(\frac{\lambda'_{2,\phi}}{\lambda'_l}\right)\left(\frac{\lambda'_l}{\lambda'_g}\right)(\overline{\rho}+\overline{\rho}_l)\frac{\partial\theta}{\partial\xi}\right] + A_{lg}Q_{dg}\exp\left\{-\frac{E'_d}{\mathcal{R}'_uT'_o}\left[1+\theta\left(\frac{T'_\infty}{T'_o}-1.0\right)\right]^{-1}\right\} + \frac{\omega_{c,F}Q_c}{\rho_g} + \frac{p}{(\overline{\rho}+\overline{\rho}_l)}\left[\frac{\partial\phi}{\partial\eta} - \xi\frac{\dot{v}_s}{v_s}\frac{\partial\phi}{\partial\xi} - \frac{3}{\psi_s}r^2(\overline{\rho}+\overline{\rho}_l)v_r\frac{\partial\phi}{\partial\xi}\right] \tag{20}$$

Eq. (18) is solved only within the droplet to obtain values of v_r for the pressure source term in Eq. (20). Eq. (19) is solved only for the gas film surrounding the droplet because liquid-phase mass diffusion is neglected. The evaluation of A_{lg} is discussed below. $\phi = 1$ outside of the droplet because no bubbles exist there. Hence the equation for θ in the gas film surrounding the droplet does not have the last two source terms in Eq. (20). Note also that the product $\rho_{g,*}Le_g$ appears rather than the term $\hat{Le}$ used by Schiller *et al.* (1996) because $\rho'_g\mathcal{D}'$ is assumed constant.

The nondimensional fuel consumption rate due to gas-phase oxidation is

$$\omega_{c,F} = k_c\rho^2Y_FY_{O_2}\exp(-E'_c/\mathcal{R}'_uT') \tag{21}$$

where $k_c = k'_c\rho'_lr'^2_o/\mathcal{D}_*$. The base case values of the nondimensional oxidation coefficients are $k_c = 2.16\times10^{10}$ ($r'_o = 1$ mm and $\mathcal{D}_*$ evaluated at 1000 K), $E'_c/\mathcal{R}'_uT'_o = 50.4$, and $Q_c = Q'_c/[C'_p(T'_\infty - T'_o)] = 58$.

The rate of change of bubble radius is given by

$$\frac{\partial R_b}{\partial\eta} = \frac{G}{\rho_g} - \frac{R_b}{3\rho_g}\frac{d\rho_g}{d\eta} + \xi\frac{\dot{\psi}_s}{\psi_s}\left(\frac{\partial R_b}{\partial\xi} + \frac{R_b}{3\rho_g}\frac{\partial\rho_g}{\partial\xi}\right) \tag{22}$$

where

$$G \equiv k_d\exp\left\{-\frac{E'_d}{\mathcal{R}'_uT'_o}\left[1+\theta\left(\frac{T'_\infty}{T'_o}-1.0\right)\right]^{-1}\right\}$$

In nondimensional form, the number of bubbles per unit mass, assumed uniform and constant, is

$$\frac{N}{m} = \frac{N\rho'_lr'^3_o}{m'} = \frac{n}{\overline{\rho}+\overline{\rho}_l} = \text{constant}$$

Combining equations (9) and (10) with $\overline{\rho} \equiv \phi\rho'/\rho'_l$ and $\overline{\rho}_l \equiv 1-\phi$ yields

$$\phi = \left(\frac{4\pi}{3}\right)\left(\frac{N}{m}\right)R_b^3(\overline{\rho}+\overline{\rho}_l) = \left[\left(\frac{4\pi}{3}\right)\left(\frac{N}{m}\right)R_b^3\right]\Big/\left[1+\left(\frac{4\pi}{3}\right)\left(\frac{N}{m}\right)R_b^3(1-\rho)\right] \tag{23}$$

The boundary conditions are $\partial\theta/\partial\xi = 0$ at $\xi = 0$, and $\theta = 1$, $Y_F = \partial Y_P/\partial r = 0$, and $Y_{O_2} = Y_{O_2,\infty}$ (0.23, unless otherwise specified) at $\xi\to\infty$.

Composite properties are used at the grid interfaces (Patankar, 1980), so only boundary conditions for Y_i are required at the interface between the liquid droplet and the gas phase.

The following mass flux balances are used for the interface boundary conditions for the species mass fractions:

$$\left(\frac{\partial Y_F}{\partial r}\right)_s = -\frac{(1-Y_F)}{3(\overline{\rho}+\overline{\rho}_l)_s r_s^2}\frac{d\psi_s}{d\eta} \tag{24a}$$

and, for oxygen and products,

$$\left(\frac{\partial Y_i}{\partial r}\right)_s = \frac{Y_i}{3(\overline{\rho}+\overline{\rho}_l)_s r_s^2}\frac{d\psi_s}{d\eta} \tag{24b}$$

Decomposition Model

In this section, equations are derived for A_{lg} and $\dot{\iota}_s$ due to (1) gasification of the droplet surface, (2) connecting of bubbles, and (3) escape of gas inside a bubble due to droplet surface regression. Let $\dot{\iota}_l$ denote the droplet mass loss rate (divided by 4π) due to decomposition and $\dot{\psi}_g$ denote the droplet mass loss rate from gas that escapes due to regression of the droplet surface. If the ratio of the two corresponding volumetric loss rates is the same as the ratio of the gas and liquid volumes, then $\dot{\psi}_l$ and $\dot{\psi}_g$ are related by

$$\dot{\psi}_g = \dot{\psi}_l \frac{\phi}{1-\phi}\frac{\rho_g'}{\rho_l'} = \dot{\iota}_l \frac{\overline{\rho}}{\overline{\rho}_l} \tag{25}$$

and $\dot{\psi}_s = \dot{\psi}_l + \dot{\iota}_g$. $\dot{\psi}_l$ is related to the individual liquid/gas interface areas that contribute to droplet mass loss by mechanisms (1) and (2) above by

$$\dot{\psi}_l = \frac{3}{4\pi}\sum_i A_i G_i \tag{26}$$

where G_i is the temperature-dependent gasification rate for each region i. The factor of 3 appears because the reference values for m and ψ are different.

Consider a spherical layer of thickness $\delta = R_b$ just below the droplet surface. Bubbles that lie partially in this layer intersect the droplet surface and gasify directly to the surrounding gas film. If the fraction of droplet surface area intersected by the bubbles is ϕ (evaluated just below the droplet surface), then the droplet surface area that gasifies is $A_1 = 4\pi r_s^2(1-\phi)$. If we further assume that any polar angle of intersection on the bubble is equally probable, then on average an intersecting bubble has a surface area of $2\pi R_b^2$ that decomposes below the droplet surface. The total decomposing surface area of all the bubbles that intersect the droplet surface can be shown to be $A_2 = 12\pi r_s^2\phi$. If bubbles do not connect below this thin subsurface layer, then $\dot{\psi}_l$ is determined from Eq. (26) using areas A_1 and A_2 with G for these regions calculated with θ_s.

Bubble connecting occurs when the void fraction exceeds a critical packing value, ϕ_c. For simply packed spheres, $\phi_c = \pi/6$, while $\phi_c = 0.7405$ for hexagonal packing. If the bubbles are not spherical in reality, then larger values of ϕ_c are possible. If we assume that the total bubble surface area is reduced by a weighting factor $\beta \leq 1$ due to bubble connecting, then $A_{lg} = 4\pi R_b^2(N/m)\beta$ is used in Eq. (20) for grid points with $\phi \geq \phi_c$.

whereas $A_{lg} = 4\pi R_b^2(N/m)$ for grid points with $\phi < \phi_c$. One exception to this is the first subsurface grid below the droplet surface (i=IDROP), where the number of bubbles that do not intersect the droplet surface is

$$\frac{4\pi}{3}\left(\frac{N}{m}\right) v_s \Delta\xi_i - 4\pi\left(\frac{N}{m}\right)(\overline{\rho} + \overline{\rho}_l) r_s^2 R_b$$

For i=IDROP, the chemical source term in Eq. (20) includes the heat release due to the decomposition of areas A_1 and A_2 as well as from the bubbles that do not intersect the droplet surface.

If the bubbles connect with each other and with the droplet surface, then gasification within the bubble can contribute to $\dot{v}_l$. In the present model, once ϕ reaches ϕ_c, all gas that decomposes in the bubble is assumed to cross the interface of the droplet and go into the gas phase. Therefore, the gasification source term is omitted from Eq. (22) for all grid points with $\phi \geq \phi_c$, and the contribution to $\dot{v}_l$ is determined from Eq. (26) using $A_{lg,i}$, G_i and $\Delta\xi_i$ for each of these grid points.

In the model without droplet surface decomposition, the governing equations were solved in a (τ, ψ) coordinate system, and the mass of the droplet was assumed to decrease by discontinuous bubble bursting at the droplet surface when $\phi \geq 1 - \epsilon$, where $\epsilon = 10^{-7}$. (Results were insensitive to ϵ providing ϵ was less than approximately 10^{-5} or 10^{-6}.) The small number ϵ was used to convert a region of nearly all bubbles into gas film. The grid points remained fixed in the ψ coordinate system, and the location of the droplet surface was defined to be the outermost point at which $1 - \phi \geq \epsilon$. This model will be referred to herein as the "(τ, ψ)" model, and the model with droplet surface decomposition will be referred to as the "(η, ξ)" model. The important differences, however, are in the physics of the decomposition model and not in the coordinate transformations.

SOLUTION PROCEDURE

We assume that a pure liquid droplet of initial temperature $\theta_o = 0$ is injected into air at pressure p' and at temperature θ_∞. The calculation proceeds in an iterative manner for the dependent variables Y_i, θ, v_r (velocity), and R_b (bubble radius). Other quantities such as void fraction, gasification rate, and densities are determined as a function of these dependent variables.

The coupled governing equations are solved numerically using a semi-implicit, finite-difference scheme that is accurate to second order in space and first order in time (Patankar, 1980). The solution procedure for each time step follows. The gasification rate crossing the droplet surface, $\dot{\psi}_s$, is calculated and ψ_s is updated. Eqs. (18)-(23) are then solved to determine, in sequential order, R_b and ϕ at each point in the droplet (after which thermal conductivities and densities are updated and source terms for the energy equation are calculated), θ, Y_i (in the gas film surrounding the droplet), and v_r in the droplet. The above steps are repeated until all dependent variables converge. The radius at each point is then updated using the nondimensional form of Eq. (16).

The energy and species equations are considered converged if the greatest change in the value of a dependent variable from one iteration to the next is less than 0.1% of the value of the variable. Excellent convergence is typically obtained in only two iterations. Numerical

results differ by less than 1% when the time step and/or mesh size are varied by a factor of two.

The radius of the outer boundary in the gas phase decreases with time if ξ(IMAX) is fixed. For simulations with the effects of gas-phase oxidation, to avoid the numerical problem of having the flame reach the outer boundary of the gas phase, after each time step the gas-phase grid is adjusted so that ψ(IMAX)=50 is fixed. This value is sufficient to keep the flame away from the outer boundary throughout a simulation. Linear interpolation is used to map the field variables in the gas phase from the old to the new grid. There is no noticeable difference in results between the model with this grid shift and results without this grid shift technique for the cases of (1) no gas-phase oxidation, and (2) with gas-phase oxidation for times at which the flame radius does not reach the outer boundary.

Simulations which did not include oxidation were terminated when $\eta = \eta_{d,*}$ (the droplet lifetime, when 99% of the initial droplet mass has gasified). For simulations with oxidation, decomposition was artificially terminated at $\eta = \eta_{d,*}$ rather than converting the remaining liquid to gas because the mass coordinate is normalized by ψ_s. These cases were terminated when either $\eta = \eta_{c,*}$ (the time at which 99% of the initial droplet mass has oxidized) or the total nondimensional oxidation rate (integrated over the gas phase) decreased to below 10^{-} after the droplet fully decomposed. The latter condition is met if the flame extinguishes before all the fuel has oxidized.

In the resolution of the large gradients near the droplet surface, the nonlinear relation between the coordinate ξ and the radial coordinate mandates the use of a nonuniform grid for ξ. A cubically increasing mesh $\xi_{n_k} = n_k^3 \Delta\xi$, where n_k is the grid point number, is employed. One exception to this formula is the first grid point outside the droplet, where $\Delta\xi$(IDROP+1) = $\Delta\xi$(IDROP)$\rho_g(\theta = 0)$ is used to resolve the initial heat fluxes at both sides of the droplet surface. Input parameters include the number of mesh points in the liquid droplet, IDROP (which determines $\Delta\xi$), and the total number of mesh points. To get at least one bubble site in the first control volume surrounding the center of the droplet, one must have IDROP $\geq 1 + (N/m)^{1/3}$.

Most of the simulations were run with 101 grid points in the droplet, 201 grid points in the gas phase, and a time step $\Delta\eta = 10^{-3}$. Results are insensitive to near factor of two changes in time step or number of grid points. All runs were performed on a DEC Alpha 5000/200 workstation. A grid dependency check was made by fixing the radius of the outer numerical boundary, R(IMAX), and using a constant value of Δr_g. Results (e.g., R_{fl} and θ_{fl} versus η) do not change appreciably if: (1) Δr_g or $\Delta\eta$ is decreased by a factor of 20, or (2) the number of grid points in the droplet is decreased by 30%.

RESULTS AND DISCUSSION

Results of parametric studies with and without gas-phase oxidation are presented separately below. Unless otherwise specified, all of the calculations reported herein used T'_o = 300 K, T'_∞ = 1000 K, $C'_p = 10^3$ J/(kg·K), p' = 1 atm, $Le_g = 0.87$, and $\mathcal{J} = 1$.

A. Results Without Gas-Phase Oxidation

The important parameters that we have studied are k_d, Q_d, N/m, λ'/λ'_l, $E'_d/(\mathcal{R}'_u T'_o)$,

p', ϕ_c, and β. The effects of these parameters on the decomposition rate and the liquid temperature distribution are discussed below.

Simplified scaling can be used to compare with the detailed computational results and predict the effect of various parameters on the characteristic time $\eta_{d,*}$ for the droplet to decompose. Taking the chemical rate control limit in which R_b increases only due to gasification, Eq. (22) gives

$$R_b \sim \rho_g^{-1} k_d \exp\left(-\frac{E_d'}{\mathcal{R}_u' T_o' \theta_*}\right) \eta \tag{27}$$

where the unknown constant $\theta_* \geq 1$ and accounts for gasification at a temperature higher than T_o'.

Substitution of Eq. (27) into Eq. (23) and scaling $\eta \rightarrow \eta_{d,*}$ when $\phi \rightarrow 1$ yields

$$\eta_{d,*} \sim \left(\frac{4\pi}{3}\frac{N}{m}\right)^{-1/3} k_d^{-1} \rho_g^{2/3} \exp\left(\frac{E_d'}{\mathcal{R}_u' T_o' \theta_*}\right) \tag{28}$$

Eq. (28) can also be obtained by scaling $\partial\theta/\partial\eta$ with the heat release due to chemical decomposition and $\theta \rightarrow Q_c$ as $\eta \rightarrow \eta_{d,*}$. In the following, the droplet lifetime $\eta_{d,*}$ is defined as the time at which 95% of the initial droplet mass has decomposed. In terms of dimensional variables, the above scaling indicates that, in the chemical limit, $\eta_{d,*}'$ is independent of the initial droplet radius, r_o'.

At $\eta = 0$, the droplet loses mass only due to gasification of the droplet surface at the initial rate of $\dot{\psi}_l = 3k_d \exp[-E_d'/(\mathcal{R}_u' T_o')]$. The time η_1 at which the rate of droplet mass loss due to gasification of the droplet surface equals the rate of mass loss due to decomposition of bubbles that intersect the droplet surface can be obtained by equating the areas A_1 and A_2 defined above (see section entitled "Decomposition Model") and by assuming that G is the same for these areas. Thus η_1 is equal to the time at which $\phi = 1/4$, which from Eqs. (23) and (27) is

$$\eta_1 \approx \left[\frac{1}{4\pi(N/m)}\right]^{1/3} \frac{\rho_g(\text{at } \theta = 0)}{k_d \exp[-E_d'/(\mathcal{R}_u' T_o')]} \tag{29}$$

If $\theta_* = 1$ in Eq. (28), then $\eta_1/\eta_{d,*} = (3\rho_g)^{-1/3} \approx 0.07$. For all the parameters investigated below, Eq. (29) correctly predicts η_1 within a factor of two or less. Using Eq. (28) with $\theta_* = 1$ tends to overpredict $\eta_{d,*}$ by about a factor of two for $\phi_c = 0.99$ and underpredict $\eta_{d,*}$ by about a factor of two for $\phi_c = \pi/6$ for $p' = 1$ atm.

Results of Base Case

The following parameters were selected for the base case: $k_d = 10^{-4}$, $Q_d = 3$, $N/m = 10^6$, $\lambda'/\lambda_l' = 0.2$, $p' = 1$ atm ($p = 1.1 \times 10^{-4}$), and $E_d'/(\mathcal{R}_u' T_o') = 4.6$. The base case value of Q_d is approximately one order of magnitude less than the heat of combustion for a hydrocarbon fuel. This value is representative of a strained hydrocarbon such as benzvalene. The heat released due to liquid-phase decomposition in this case causes the flame temperature of an energetic liquid fuel to be approximately 10% greater that that of a hydrocarbon. In the absence of any definitive data in the literature, we selected $E_d'/(\mathcal{R}_u' T_o') = 4.6$ so that the value of E_d' is one order of magnitude lower than the activation energy for gas-phase kinetics

of hydrocarbon fuels and is of the same order of magnitude as the product of M_F and a typical hydrocarbon latent heat of vaporization. Note that, for conventional hydrocarbons, this product is effectively an activation energy for vaporization. The number of bubbles per mass, N/m, was selected so as to have at least one bubble site in the smallest computational control mass. Eq. (28) with the base case values and ρ_g evaluated at 650 K gives $\eta_{d,*} = 35$. This value of $\eta_{d,*}$ is one order of magnitude less than the nondimensional droplet lifetime predicted by the classical d^2-Law for hydrocarbon droplets vaporizing in a non-oxidizing, 1000 K, 1 atm environment (Kanury, 1975).

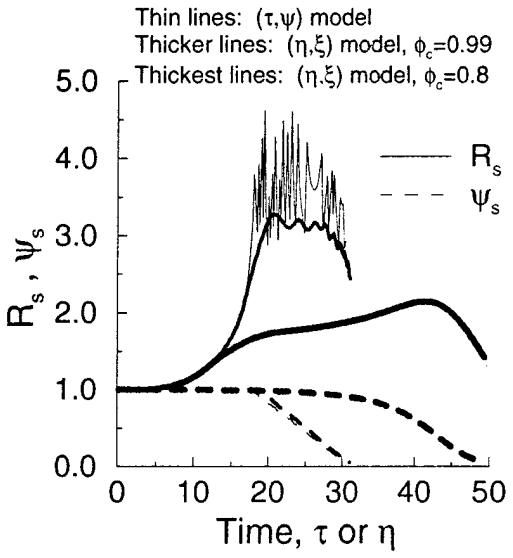

Figure 3: Variation of radius and mass coordinate at the droplet surface for the (τ, ψ) model without droplet surface decomposition and the (η, ξ) model with droplet surface decomposition using data for the base case: $k_d = 10^{-4}$, $Q_d = 3$. $N/m = 10^6$, $\lambda'/\lambda'_l = 0.2$, $p' = 1$ atm. and $E'_d/(\mathcal{R}'_u T'_o) = 4.6$. Two values of ϕ_c are shown for the (η, ξ) model.

Figure 3 shows a comparison of r_s and ψ_s versus time for the two models using the base case parameters. After $\phi \to 1$ with the (τ, ψ) model without droplet surface decomposition, the intermittent bursting of bubbles into the gas film causes small oscillations of the droplet radius as it intermittently swells (due to sensible heating of the bubbles) and shrinks (due to the bubble bursting). Conversely with the (η, ξ) model with droplet surface decomposition, the droplet radius continuously increases with time until surface decomposition becomes appreciable, after which time the droplet mass and droplet radius decrease continuously with time.

Figure 4 shows radial profiles of temperature at different times obtained from the (η, ξ) model for the base case with $\phi_c = 0.99$. The results are similar to those from the (τ, ψ) model. The nondimensional temperature does not exceed unity until the void fraction just below the liquid surface exceeds approximately 0.9. The energy released due to the decomposition causes the temperature to peak near the droplet surface with $\theta_{\max} \to Q_d$. A comparison of the individual terms in the energy equation indicates that the rate of temperature increase, $\partial\theta/\partial\eta$, just below the droplet surface is due primarily to conduction at $\eta = 10$. At $\eta = 15$,

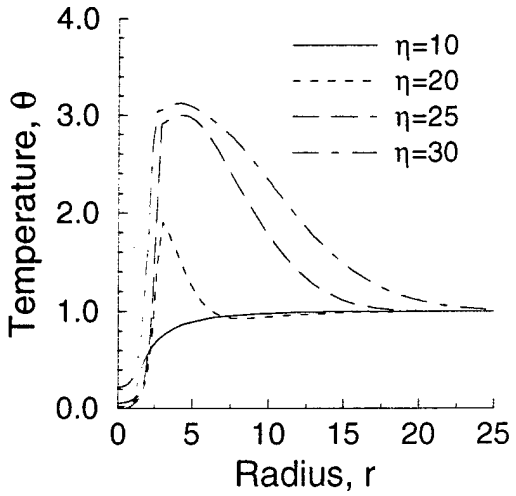

Figure 4: Radial profiles of temperature at different times obtained from the (η, ξ) model for the base case with $\phi_c = 0.99$.

conduction and the heat release due to decomposition contribute more or less equally to the rate of temperature increase just below the droplet surface. For $\eta \geq 20$, the heat due to decomposition is much greater than the heat conduction throughout the droplet. The source term due to the moving boundary is typically negative for $\xi < 1$, negligible for $\eta \leq 10$, and of the same order as the chemical decomposition term in the region $0.5 \leq \xi \leq 0.9$ for $\eta \geq 20$. At all times and radial positions, the pressure term in the energy equation is negligible.

Effects of ϕ_c, 3 and p'

As the critical packing value, ϕ_c, is decreased in the (η, ξ) model, the droplet radius increases more gradually, the maximum value of r_s decreases, and the time for the droplet to decompose fully increases. For example, $\eta_{d,*} = 31$ for $\phi_c = 0.99$, $\eta_{d,*} = 49$ for $\phi_c = 0.8$, and $\eta_{d,*} = 85$ for $\phi_c = \pi/6$. These effects are due to the reduction in the rate of increase of R_b and hence ϕ when $\phi \geq \phi_c$ (see Fig. 5) because the mass of gas in the bubbles is assumed fixed (gas that decomposes along the surface of the bubbles leaves the droplet) when $\phi \geq \phi_c$. Figures 3 and 5 show that the results of the (τ, ψ) and (η, ξ) models are in good agreement (with the exception of the oscillations in r_s) in the limit where $\phi_c \to 1$. The radial profiles of temperature for the (η, ξ) model with base case data and $\phi_c = 0.8$ are similar to Fig. 4 except $\theta_{\max}$ increases to about 7.0 near the droplet surface when the droplet is almost completely decomposed. Although the (η, ξ) model agrees well with the (τ, ψ) model for $\phi_c = 0.99$ and also predicts a value of $\eta_{d,*}$ that agrees fairly well with Eq. (28), bubbles probably connect before ϕ reaches 0.99. Therefore, the following results are presented for the (η, ξ) model with $\phi_c = 0.8$.

Figure 6 shows the nondimensional rate of mass loss (divided by 4π) at the droplet surface, $\dot{\psi}_s = -d\psi_s/d\eta$, versus time for the base case. As discussed above, the droplet loses mass due to: gasification of the droplet surface (proportional to A_1), decomposition of bubbles that connect with the droplet surface (including the bubbles in the subsurface layer of thickness $\delta = R_b$), and gas loss due to droplet surface regression. The gasification

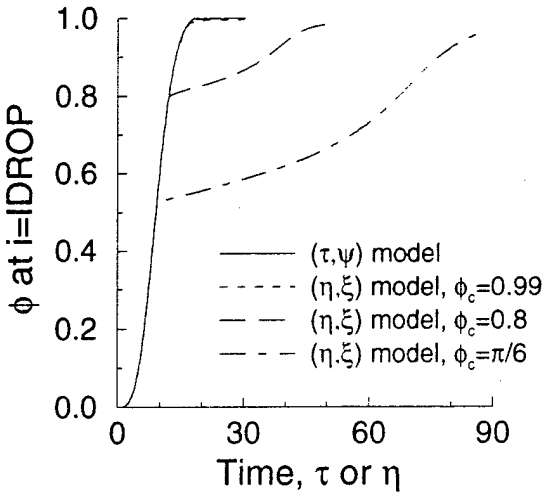

Figure 5: Variation of void fraction just below the droplet surface (i=IDROP) for (τ, ψ) and (η, ξ) models using data for the base case. Different values of ϕ_c are shown for the (η, ξ) model.

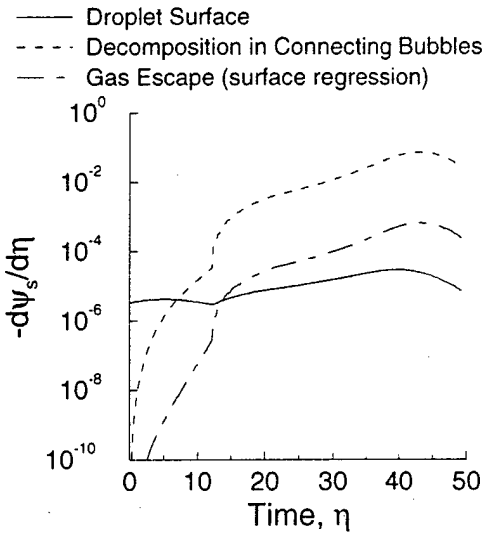

Figure 6: Nondimensional rate of mass loss (divided by 4π) at the droplet surface, $\dot{\psi}_s = -d\psi_s/d\eta$, versus time for the base case with $\phi_c = 0.8$.

rate of the droplet surface varies by less than one order of magnitude throughout the droplet lifetime. Droplet mass loss due to gasification from bubbles that connect with the droplet surface exceeds the droplet surface gasification rate at $\eta = 7.0$, which is approximately 14% of the droplet lifetime. The mass loss rate due to bubbles connecting with the droplet surface increases sharply when $\phi(i{=}\text{IDROP})$ reaches ϕ_c (at $\eta = 12.4$), and exceeds the droplet surface gasification rate by more than three orders of magnitude for $\eta > 0.5\eta_{d,*}$.

Decreasing β [through A_{lg} in Eq. (20)] below unity increases $\eta_{d,*}$ but does not change qualitatively the radial profiles of θ, R_b, etc.

Eqs. (28) and (6) predict that $\eta_{d,*} \propto p^{2/3}$. The numerical results indicate that $\eta_{d,*}$ increases more weakly with ambient pressure. For $p' = 0.2$ atm, we find $\eta_{d,*} \propto p^{0.12}$ whereas $\eta_{d,*} \propto p^{0.26}$ for $p' = 10$ atm. For all the parameters studied, the temperature peaks near the droplet surface after the droplet has decomposed appreciably. As shown by Figure 7b, the gas-phase temperature decays more gradually with r at lower p'.

Effects of Other Nondimensional Parameters

The nondimensional equations reveal that the most relevant nondimensional parameters in this problem are N/m, k_d, Q_d, λ'/λ'_l, and $E'_d/(\mathcal{R}'_u T'_o)$. The nondimensional parameter T'_∞/T'_o was not investigated for the case of no gas-phase oxidation. Radial temperature profiles corresponding to the times at which 50% of the initial liquid mass has decomposed and the decrease in droplet mass relative to the initial droplet mass as a function of time are shown in Figures 7 and 8, respectively, for the above parameters. Figure 8 shows that, for all cases except $Q_d = 1$ and $k_d = 2.5 \times 10^{-5}$, the droplet gasifies very quickly after approximately 20% of the initial liquid mass has decomposed.

The number of bubbles per unit mass, N/m, directly affects the void fraction [Eq. (23)]. Results indicate that $\eta_{d,*}$ decreases with increasing N/m. Consistent with Eq. (28), $\eta_{d,*}$ is proportional to approximately $(N/m)^{-1/3}$ for $N/m > 10^8$. For much smaller N/m (e.g., $N/m = 10^4$), $\eta_{d,*} \propto (N/m)^{-0.23}$, indicating a small deviation from the chemical limit. As N/m increases, the peak temperature corresponding to the times at which 50% of the initial liquid mass has decomposed increases and the temperature distribution in the droplet becomes less uniform because less time is available for heat to conduct through the droplet (Fig. 8b).

The nondimensional rate constant, k_d, can be viewed as a modified Damköhler number because it is proportional to the ratio of the decomposition rate constant to the diffusion rate. Although decomposition occurs in the liquid phase while the diffusivity in the denominator of k_d is for the gas phase, varying k_d is equivalent to varying the decomposition rate for fixed values of the other parameters. Consistent with the scaling analysis [Eq. (28)], the decomposition rate is very sensitive to k_d. For large N/m and relatively large k_d (e.g., $k_d \geq 10^{-4}$), the numerical model predicts that $\eta_{d,*}$ is approximately proportional to $k_d^{-1}(N/m)^{-1/3}$ in agreement with Eq. (28). If $\eta_{d,*} \propto k_d^a (N/m)^b$, then defining $\alpha \equiv -(a+3b)$, the dimensional droplet lifetime varies with initial droplet radius as $\eta'_{d,*} \propto r_o'^{2-\alpha}$. The chemical limit [Eq. (28)] is $\alpha = 2$ while the diffusion limit is $\alpha = 0$. Figure 9 summarizes the effect of k_d and N/m on the dependence of droplet lifetime $\eta'_{d,*}$ on the initial droplet radius. The diffusion limit $\alpha = 0$ is not predicted by the present model because the droplet is assumed to lose mass solely due to decomposition and not due to a phase-equilibrium relationship.

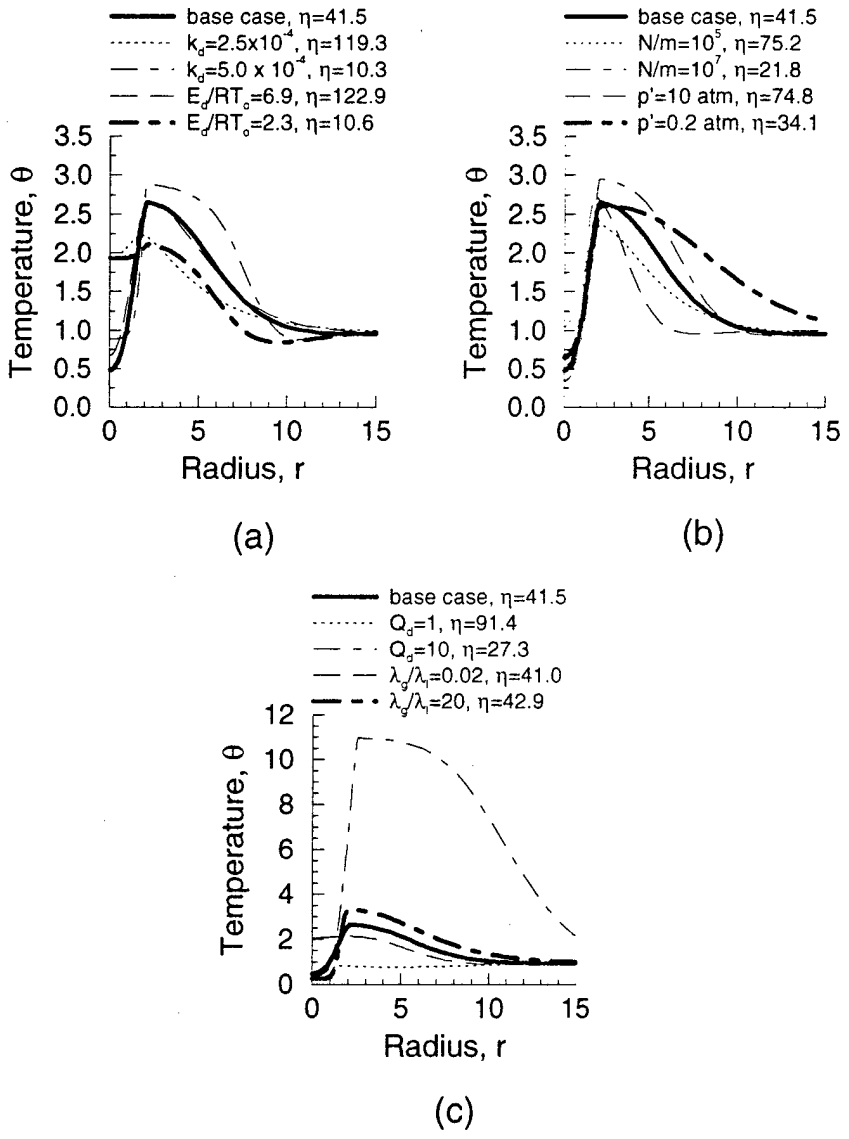

Figure 7: Effect of parameters on the radial profiles of temperature ($\phi_c = 0.8$) at times corresponding to 50% droplet mass loss. The base case is $k_d = 10^{-4}$, $Q_d = 3$, $N/m = 10^6$, $\lambda'/\lambda'_l = 0.2$, $p' = 1$ atm, and $E'_d/(\mathcal{R}'_u T'_o) = 4.6$.

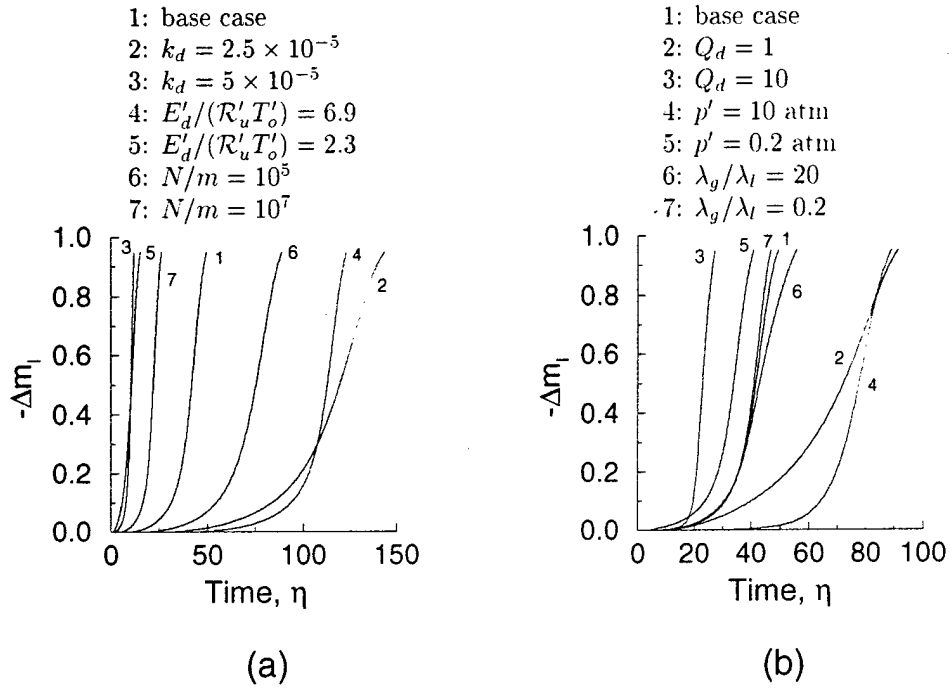

Figure 8: Decrease in droplet mass relative to the initial droplet mass, $-\Delta m_l$, as a function of time for the parameters k_d, $E'_d/(\mathcal{R}'_u T'_o)$, N/m, Q_d, p', and λ'/λ'_l.

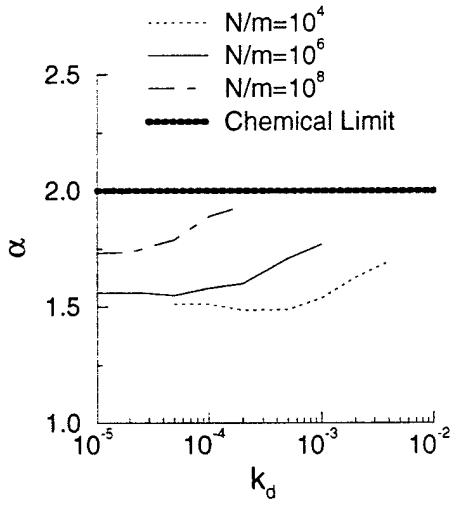

Figure 9: Dependence of droplet lifetime $\eta'_{d,*}$ on the initial droplet radius r'_o; $\eta'_{d,*} \propto r'^{2-\alpha}_o$. The chemical limit is $\alpha = 2$ while the diffusion limit is $\alpha = 0$.

As k_d decreases, the peak temperature $\theta_{\max}$ decreases and θ becomes more uniform in the droplet (Fig. 7a). Like the parameter k_d, the nondimensional activation energy, $E'_d/(\mathcal{R}'_u T'_o)$, directly affects the gasification rate. The droplet lifetime depends more strongly on $E'_d/(\mathcal{R}'_u T'_o)$ for smaller values of $E'_d/(\mathcal{R}'_u T'_o)$ (i.e., closer to the chemical limit). For $\phi_c = 0.8$, the dependence of $\eta_{d,*}$ on $E'_d/(\mathcal{R}'_u T'_o)$ varies between $\eta_{d,*} \propto e^{0.4E'_d/(\mathcal{R}'_u T'_o)}$ and $\eta_{d,*} \propto e^{0.5E'_d/(\mathcal{R}'_u T'_o)}$ for $2.3 \leq E'_d/(\mathcal{R}'_u T'_o) \leq 6.9$. For $\phi_c = 0.99$, this dependence varies between $\eta_{d,*} \propto e^{0.48E'_d/(\mathcal{R}'_u T'_o)}$ and $\eta_{d,*} \propto e^{0.76E'_d/(\mathcal{R}'_u T'_o)}$. Although decreasing $E'_d/(\mathcal{R}'_u T'_o)$ or increasing k_d increases $\eta_{d,*}$, the temperature profile for a relatively small value of $E'_d/(\mathcal{R}'_u T'_o) = 2.3$ is relatively uniform and similar to the case of a value of k_d that is smaller than the base case value (Fig. 7a). For smaller k_d, the more uniform temperature profile is due to the increased role of conduction whereas for smaller $E'_d/(\mathcal{R}'_u T'_o)$ the more uniform θ profile is due to the lower activation temperature required for appreciable chemical reactions.

According to Eq. (28), Q_d affects the characteristic time for droplet decomposition only indirectly through the evaluation of ρ_g and θ_*. As Q_d increases, gasification occurs at a higher temperature and also ρ_g decreases. Substituting $\rho_g \propto Q_d^{-1}$ and a value of θ_* greater than unity into Eq. (28) would result in a dependence of $\eta_{d,*}$ on Q_d stronger than $\eta_{d,*} \propto Q_d^{-2/3}$. Decomposition, however, occurs very rapidly once $\phi \to \phi_c$ near the droplet surface. Throughout the liquid, $\theta_l \leq 1$ for the majority of the time before the droplet is fully decomposed (see Fig. 4). Therefore, the model predicts that $\eta_{d,*}$ has a weaker dependence on Q_d (approximately $\eta_{d,*} \propto Q_d^{-1/2}$). For all the parameters investigated, $\theta_{\max} \approx Q_d$ at the time when 50% of the initial liquid mass has decomposed (Fig. 7).

The gas-phase thermal conductivity, λ', appears in the parameter Le_g, which is not varied in the parametric study. Therefore, changing the ratio of the thermal conductivities, λ'/λ'_l, is essentially the same as varying λ'_l. Increasing λ'/λ'_l (e.g., by decreasing the liquid-phase thermal conductivity) increases slightly the overall time for decomposition (Fig. 8b) because heat conducts through the droplet more slowly. Increasing λ'/λ'_l also results in a more peaked temperature profile near the droplet surface (Fig. 7c) because of the reduced heat conduction in the droplet.

B. Results With Gas-Phase Oxidation

The ignition delay time and flame propagation rate are influenced by the gasification rate, which is inversely proportional to $\eta_{d,*}$. Hence it will be shown that Eq. (28), derived above for the chemical rate control limit of the droplet lifetime without gas-phase oxidation, also correlates the effect of decomposition parameters on the flame behavior.

The flame location herein is defined as the point of maximum $\omega_{c,F}$. Alternative definitions such as the point of maximum Y_P do not change the position of the flame significantly. Unless otherwise specified, all of the calculations reported herein used $k_d = 10^{-4}$, $Q_d = 3$, $N/m = 10^6$, $\lambda'/\lambda'_l = 0.2$, and $E'_d/(\mathcal{R}'_u T'_o) = 4.6$. Most of the nondimensional parameters were varied by at least one order of magnitude from their base case values in the parametric study below. The following results were recently submitted for archival publication (Schiller *et al.*, 1997).

Flame Radius, Flame Temperature, and Ignition Delay

In classical droplet burning, the ratio R_{fl}/R_s asymptotically tends to a constant, and the flame radius first increases but then decreases due to the shrinking of the droplet. Similar behavior is predicted by the present model if decomposition is not considered and classical droplet vaporization boundary conditions are used at the droplet surface. Conditions at the interface in the model with decomposition, however, differs from classical droplet models in two ways: (1) the gasification rate is determined from the decomposition model rather than from the use of a Clausius-Clapeyron relation combined with a Stefan flow assumption, and (2) the gasification process is exothermic. As a result, the model predicts that the variation of flame radius with time is quite different than that of classical droplet combustion.

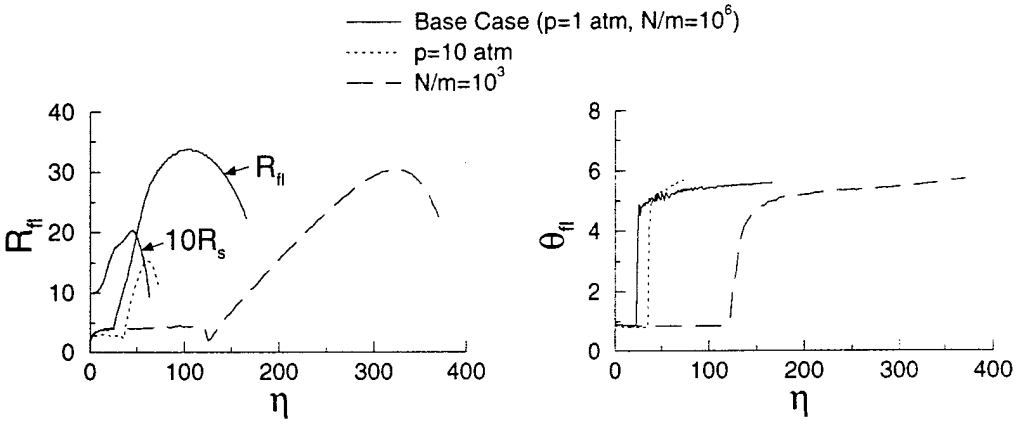

Figure 10: Flame radius and flame temperature versus time for different values of ambient pressure and number of bubbles per unit mass. The droplet radius (multiplied by 10) is also shown for the base case. The droplet lifetime, $\eta_{d,*}$, is: 63.4 (base case), 59.5 ($p' = 10$ atm), and 333.7 ($N/m = 10^3$).

Over the investigated range of the fundamental parameters, R_{fl} first increases nearly linearly with η after an ignition delay period (Fig. 10). The ignition delay time increases with decreasing gasification rate (e.g., due to a decrease in k_d or N/m), in a manner qualitatively similar to Eq. (28). Plots of R_{fl} and θ_{fl} versus η for $k_d = 10^{-5}$ and $N/m = 10^6$ are nearly identical to those shown in Fig. 2 for $k_d = 10^{-4}$ and $N/m = 10^3$. Eq. (28) predicts that a one order of magnitude decrease in $k_d =$ has the same effect on the droplet lifetime as a three order of magnitude decrease in N/m. The flame behavior thus has a qualitatively similar dependence on the parameters that affect the decomposition rate.

As η increases, the droplet radius first increases due to bubble growth, but then subsequently decreases as the droplet gasifies (Fig. 10). R_{fl}/R_s also increases with time for $\eta < \eta_{d,*}$. Unlike classical droplet burning, no simple relationship exists for the variation of R_{fl}/R_s with time. After decomposition is artificially terminated at $\eta = \eta_{d,*}$, R_{fl} increases but then subsequently decreases with η, similar to classical droplet combustion. The flame radius might vary differently with time while the droplet decomposes as compared to classical droplet combustion because the gasification rate due to decomposition is more than one order of magnitude greater than that due to classical vaporization. Apparently, the higher

gasification rate causes the flame to move away from the droplet surface more rapidly.

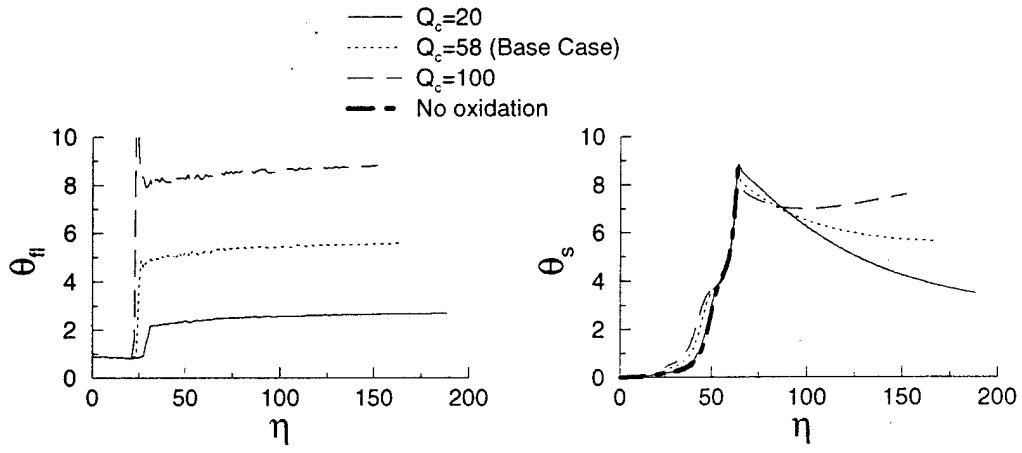

Figure 11: Flame temperature and droplet surface temperature versus time for different values of Q_c. The droplet surface temperature is also shown for the case of no gas-phase oxidation ($k_c = Q_c = 0$). $\eta_{d,*}$ varies between 63 and 64 for these cases.

Over the investigated range, parameters that directly affect only the decomposition rate (e.g., N/m, k_d, etc.) or the rate of oxidation do not appreciably change the maximum temperature in the gas phase. Figures 10 and 11 show that the flame temperature does not vary significantly with time soon after the flame is initiated. As expected, θ_{fl} is fairly insensitive to ambient pressure and increases as the amount of heat released due to gas-phase oxidation is increased. For benzene, the adiabatic flame temperature with a constant value of specific heat and $Y_{O_2,\infty} = 0.23$ is $\theta_{fl} = 1 + 0.07Q_c$, which is consistent with the model's predicted values of θ_{fl} for $Q_d = 0$ (no heat release due to decomposition). As shown by Figs. 10 and 11, the base case value of $Q_d = 3$ causes θ_{fl} to increase slightly above the adiabatic flame temperature (e.g., by approximately 6% for $Q_c = 58$). Also consistent with the theoretical values of adiabatic flame temperature for constant C_p, θ_{fl} increases from approximately 2.0 to 9.4 when $Y_{O_2,\infty}$ is changed from 0.05 to 0.46 (Fig. 12).

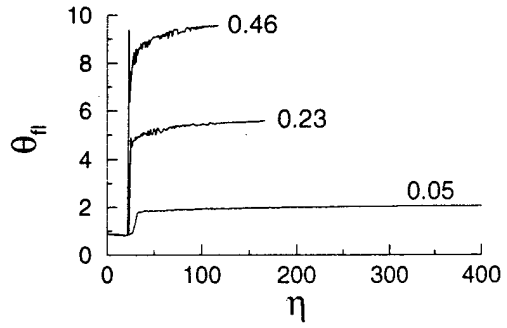

Figure 12: Flame temperature versus time for three values of $Y_{O_2,\infty}$ (curve labels).

Increasing Q_d from 0 to 5 decreases the ignition delay time from 28 to 23 (Fig. 13) and increases θ_{fl} from 5.2 to 5.7. As shown by Fig. 13, higher values of Q_d lead to greater gasification rates and thus faster flame propagation. For $Q_d = 0$, the droplet lifetime is almost equal to the time required for complete oxidation ($\eta_{d,*} = 304.8$, $\eta_{c,*} = 312.4$), whereas oxidation occurs relatively long after the droplet has fully decomposed for $Q_d = 5$ ($\eta_{d,*} = 48.0$, $\eta_{c,*} = 149.2$).

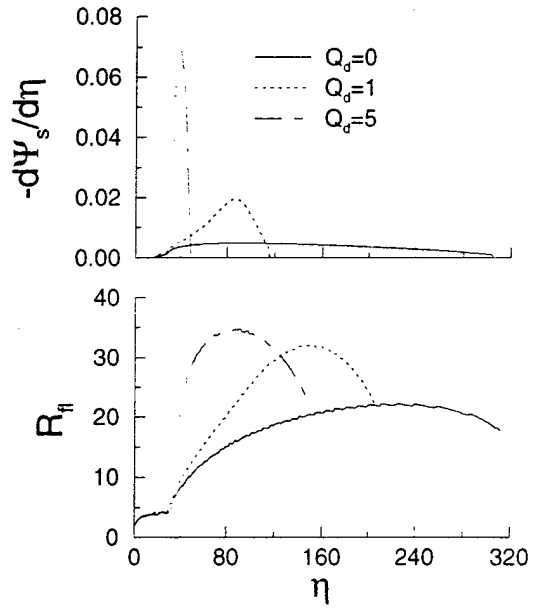

Figure 13: Flame radius and nondimensional gasification rate as functions of time for three values of Q_d.

Effect of Gas-Phase Oxidation on Droplet Lifetime

Gas-phase oxidation does not appreciably affect the droplet lifetime for: (1) the base case values of the nondimensional parameters, or (2) any variation of parameters that results in a fast rate of gasification compared to oxidation. The insensitivity of $\eta_{d,*}$ to gas-phase oxidation occurs because the droplet lifetime is governed primarily by the chemical rate control limit of liquid-phase decomposition. The temperatures in the droplet rise quickly due to the heat released by decomposition before they are affected by heating due to conduction from the flame. Gas-phase oxidation does, however, appreciably affect $\eta_{d,*}$ if the rate of decomposition is slowed significantly, thus giving more time for conduction from the flame to affect the droplet heating. Figure 14 shows the nondimensional total mass rate of gasification and oxidation as functions of time for two values of N/m. For $N/m = 10^6$ (base case value), the droplet is gasified at $\eta_{d,*} = 63.4$, whereas oxidation is not complete until $\eta_{c,*} = 166.2$. Because gasification is relatively fast compared to oxidation for the base case, gas-phase oxidation decreases $\eta_{d,*}$ by less than 1%. Conversely, for $N/m = 10^3$, decomposition occurs more slowly, thus giving more time for conduction from the flame to affect the droplet heating. Unlike the base case, at any given time the total mass that has oxidized is comparable to

that which has gasified for $N/m = 10^3$. In this case, gas-phase oxidation decreases $\eta_{d,*}$ by 16%. Plots of gasification and oxidation rates, as well as the effect of gas-phase oxidation on $\eta_{d,*}$, for $k_d = 10^{-5}$ and $N/m = 10^3$ are similar to those for $k_d = 10^{-4}$ and $N/m = 10^3$.

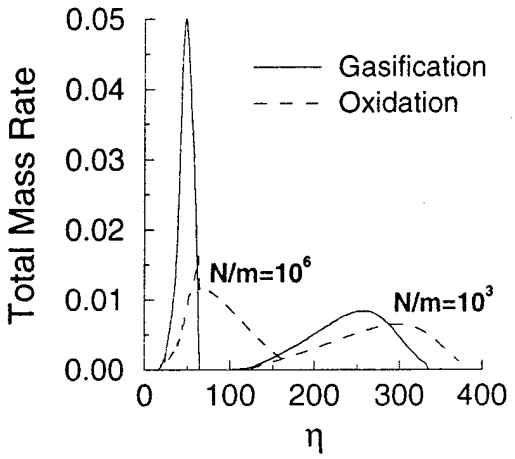

Figure 14: Total mass rate of gasification and oxidation as functions of time for two values of N/m.

As the ambient pressure increases, both the droplet lifetime and the time required for complete oxidation decrease (Fig. 10), and the ratio $\eta_{c,*}/\eta_{d,*}$ approaches unity. In general, the effect of gas-phase oxidation on the droplet lifetime decreases as $\eta_{c,*}/\eta_{d,*}$ becomes greater than unity. For example, the decrease in $\eta_{d,*}$ due to gas-phase oxidation is 19% for $p' = 20$ atm ($\eta_{c,*}/\eta_{d,*} = 1.09$), 7.5% for $p' = 10$ atm ($\eta_{c,*}/\eta_{d,*} = 1.23$), and 0.6% for $p' = 1$ atm ($\eta_{c,*}/\eta_{d,*} = 2.62$).

The droplet lifetime is insensitive to large changes in k_c, $E_c'/(\mathcal{R}_u' T_o')$, Q_c, and $Y_{O_2,\infty}$. For example, $\eta_{d,*}$ decreases by roughly 1% when either Q_c is increased from 20 to 100, $Y_{O_2,\infty}$ is increased from 0.05 to 0.46, or k_c is increased by two orders of magnitude. The insensitivity to changes in the oxidation rate constants is indicative of a fast reaction. Although Q_c and $Y_{O_2,\infty}$ affect the flame temperature, they do not appreciably change $\eta_{d,*}$ for base case values of the other parameters because the droplet lifetime is governed by liquid-phase decomposition. The plot of droplet surface temperature (θ_s) versus time in Fig. 11 indicates that the increase in flame temperature with Q_c does increase θ_s for much of the droplet lifetime. But the droplet temperature profile and thus the gasification rate are affected more by the exothermic rate of heat release due to liquid decomposition than by the increased rate of heat conduction from the flame. The insensitivity of θ_s (and θ throughout the droplet) to θ_{fl} (through Q_c) is especially evident in the last 15% of the droplet lifetime, when liquid-phase decomposition dominates the droplet heating.

As shown by Fig. 15, the droplet almost fully decomposes before one-third of the fuel has oxidized. Higher ambient temperature results in more rapid heat conduction to the droplet and more rapid exothermic gasification (decomposition) with subsequent further liquid heating. The droplet lifetime therefore decreases with an increase in T_∞'/T_o'. (T_o' was fixed at 300 K for these simulations.) Gas-phase oxidation, however, does not affect $\eta_{d,*}$

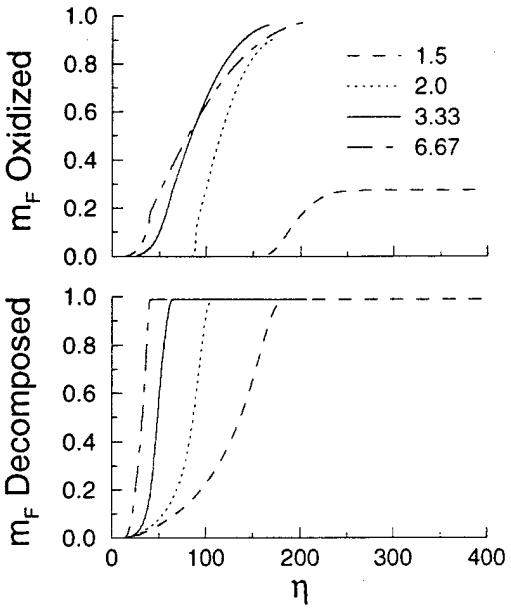

Figure 15: Total mass of fuel (m_F) oxidized and decomposed as functions of time for four values of T'_∞/T'_o.

over the investigated range of ambient temperatures ($1.1 \leq T'_\infty/T'_o \leq 6.67$). Moreover, the rapid increase of the flame radius (Fig. 10) increases the time required for heat to conduct from the flame to the droplet surface. Hence the droplet surface temperature increases more rapidly with increasing T'_∞/T'_o than with increasing flame temperature (compare Fig. 16 with Fig. 11). The heat release due to liquid-phase decomposition causes θ_s to exceed the flame temperature (Figs. 11 and 16). As shown by Fig. 16, the droplet surface temperature decreases rapidly with time soon after the liquid stops decomposing. For $T'_\infty/T'_o = 1.5$, the flame extinguishes before 30% of the initial fuel mass is oxidized. Ignition does not occur for $T'_\infty/T'_o \leq 1.2$.

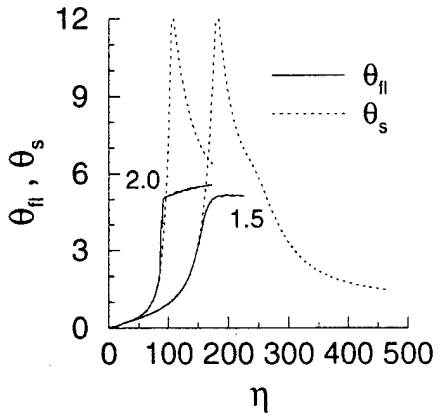

Figure 16: Flame temperature and droplet surface temperature as functions of time for $T'_\infty/T'_o = 1.5$ ($\eta_{d,*} = 180.6$, flame extinguishes) and $T'_\infty/T'_o = 2.0$ ($\eta_{d,*} = 106.0$, $\eta_{c,*} = 174.4$).

Gas-Phase Profiles

As stated above, the droplet lifetime is affected by gas-phase oxidation if the rate of liquid-phase decomposition is decreased sufficiently. The droplet lifetime is reduced by 27% due to gas-phase oxidation for $N/m = 10^2$. As shown by Fig. 17a, there is appreciable heating of the droplet by gas-phase conduction from the flame over much of the droplet lifetime because $\eta_{d,*}$ is relatively large. That is, the time scale for heat conduction from the flame to the droplet becomes comparable or even smaller than that for liquid-phase decomposition. Comparatively, for $N/m = 10^6$, the heat from the flame does not have time to conduct to the droplet surface before $\eta = \eta_{d,*}$. As shown in Fig. 17b, heat actually conducts away from the droplet surface during most of the droplet lifetime for $N/m = 10^6$. Results indicate that the speed of the flame, $dR_{\text{fl}}/d\eta$, decreases with $\eta_{d,*}$. The time required for heat to conduct from the flame to the droplet surface varies with $\sqrt{R_{\text{fl}} - 1}$. Therefore, the reduction in flame speed as $\eta_{d,*}$ is reduced contributes to the decrease in the time scale for heat conduction from the flame to the droplet. Similar to classical droplet burning, the profiles of Y_i in Fig. 17 indicate that the flame is diffusion controlled, with almost no oxygen in the region $r < R_{\text{fl}}$ and no fuel vapor in the region $r > R_{\text{fl}}$.

CONCLUSIONS

A simplified, spherically-symmetric model of the transient heating of an energetic liquid fuel droplet has been developed. The decomposition of the energetic fuel was examined for a range of nondimensional parameters including a modified Damköhler number, heat of decomposition, activation energy, number of bubbles per unit mass, and ratio of thermal conductivities.

Without the effects of gas-phase oxidation, detailed results of the base case, which were qualitatively similar to all of the simulations, revealed the following. The bubble radius grows with radial position and time, causing the droplet to swell initially. A model that incorporates decomposition of the droplet surface predicts that the droplet radius continuously increases with time until surface decomposition becomes appreciable, after which time the droplet mass and droplet radius decrease continuously with time. The time required for the droplet to decompose decreases as ϕ_c is increased or β is decreased in the model that includes droplet surface decomposition. A model that assumes the droplet mass decreases due to bubbles discontinuously bursting at the droplet surface predicts that, after $\phi \to 1$ just below the droplet surface, the intermittent bursting of bubbles into the gas film causes small oscillations of the droplet radius as it intermittently swells (due to sensible heating of the bubbles) and shrinks (due to the bubble bursting). The mean value of r_s decreases with the mass of the droplet. The results of the two models are in good agreement (with the exception of the oscillations in r_s) in the limit where $\phi_c \to 1$. The temperature peaks just outside of the droplet surface due to decomposition. Heat conduction is dominant during the early stages of droplet heating, then the chemical energy release dominates later.

Consistent with simplified scaling for the limit of chemical rate control, the characteristic time for decomposition ($\eta_{d,*}$) is strongly dependent on k_d and $E'_d/(\mathcal{R}'_u T'_o)$, and less strongly

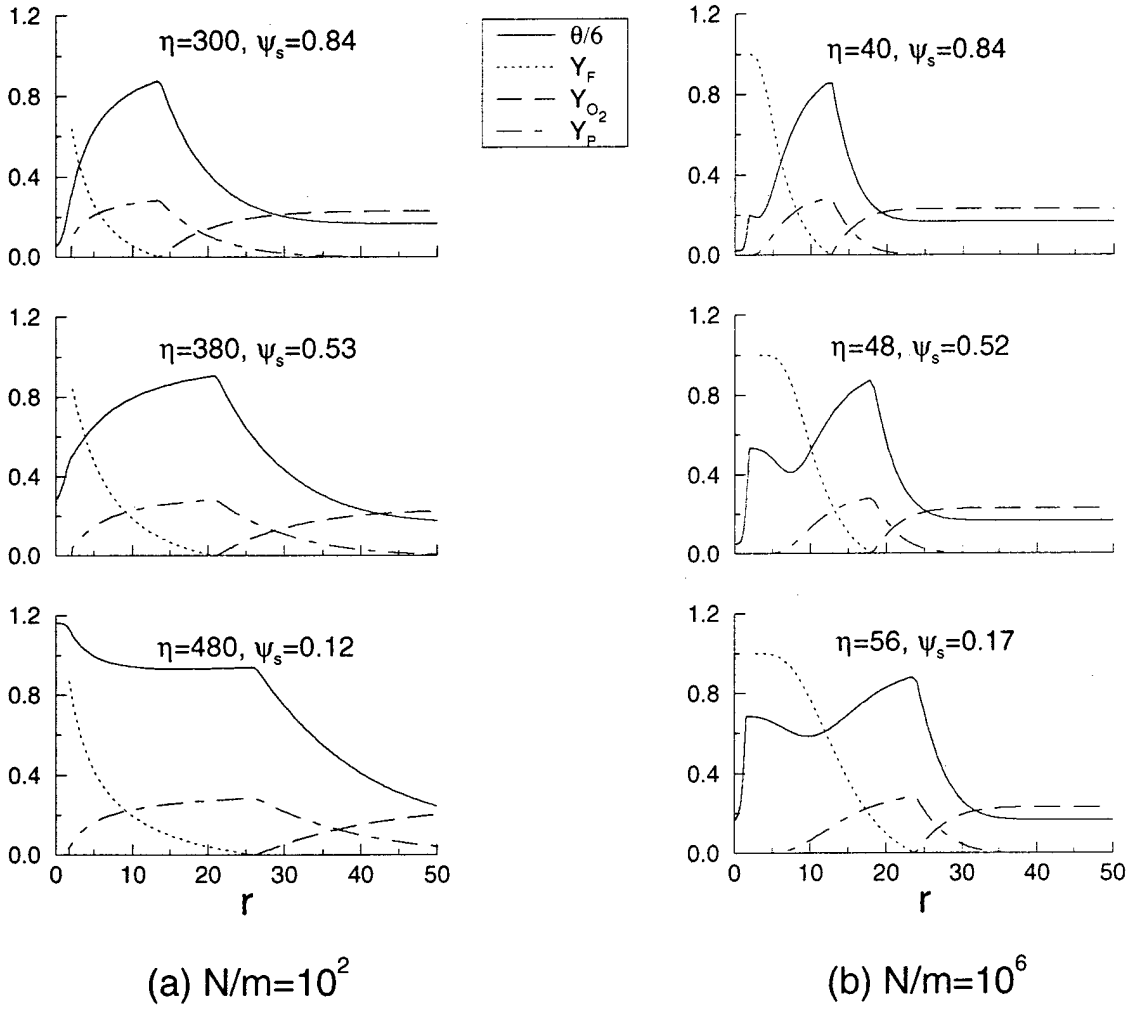

Figure 17: Gas-phase profiles of θ and Y_i at different values of η and N/m.

on N/m, p', and Q_d. Increasing λ'/λ'_l increases $\eta_{d,*}$ slightly and results in a more peaked temperature profile. Over the range of parameters investigated, $\eta'_{d,*}$ is proportional to r'_o to a power between 0.1 and 0.5, indicating that the chemical kinetic control of the droplet lifetime is stronger than the diffusion control.

With the effects of gas-phase oxidation, the flame radius is predicted to increase nearly linearly with time before subsequently decreasing. This behavior differs from classical droplet burning due to the exothermic decomposition process that determines the gasification rate. Because the ignition delay time and flame propagation rate depend on the gasification rate of the droplet (typically controlled by liquid-phase decomposition rather than gas-phase conduction), simplified scaling previously derived for the droplet lifetime also correlates the effect of decomposition parameters on the flame behavior. Decreasing the decomposition rate (e.g., by reducing k_d or N/m) increases the ignition delay time and reduces the flame propagation rate.

For the selected base case, liquid-phase decomposition increases the flame temperature by approximately 6%. Therefore, energetic liquid fuels can be expected to vaporize and burn more rapidly and to yield more thermal energy than conventional hydrocarbon fuels. The droplet lifetime for the base case, however, is not affected significantly by gas-phase oxidation because the droplet fully decomposes before heat conduction from the flame can appreciably affect the droplet heating. As the decomposition rate is reduced, the time scale for heat conduction from the flame to the droplet becomes comparable to that of liquid decomposition, and hence gas-phase oxidation significantly reduces $\eta_{d,*}$. In general, the effect of gas-phase oxidation on the droplet lifetime decreases as $\eta_{c,*}/\eta_{d,*}$ becomes greater than unity.

Gas-phase profiles of θ and Y_i for the base case ($N/m = 10^6$) indicate that: (1) the flame is diffusion controlled, (2) the flame radius increases with η, and (3) heat from the flame does not conduct into the droplet over most of the droplet lifetime. If, however, N/m is reduced to 10^2, thus slowing the decomposition rate, then there is sufficient time for heat to conduct from the flame to the droplet. In this case, gas-phase oxidation reduces the droplet lifetime by approximately 27%.

REFERENCES

Bhatia, R. and Sirignano, W. A. (1992), "Transient Heating and Burning of Droplet Containing a Single Metal Particle," *Combust. Sci. Tech.*, Vol. 84, pp. 141–162.

Brill, T. B. and Karpowicz, R. J. (1982), "Solid Phase Transition Kinetics. The Role of Intermolecular Forces in the Condensed-Phase Decomposition of Octahydro-1,3,5,7-tetranitro-1,3,5,7-tetrazocine," *J. Phys. Chem.*, Vol. 86, pp. 4260–4265.

Chervinsky, A. (1969), "Transient Burning of Spherical Symmetric Fuel Droplets," *Israel Journal of Technology*, Vol. 7, No. 1–2, pp. 35–42.

Eaton, P. E. (1992), "Cubanes: Starting Materials for the Chemistry of the 1990s and the New Century," *Angew. Chem. Int. Ed. Engl.*, Vol. 31, No. 11, pp. 1421–1436.

Hsieh, W.-H., Peretz, A., Huang, I.-T., and Kuo, K. K. (1991), "Combustion Behavior of Boron-Based BAMO/NMMO Fuel-Rich Solid Propellants," *Journal of Propulsion and*

Power, Vol. 7, No. 4, pp. 497–504.

Kanury, A. M. (1975), "Introduction to Combustion Phenomena." *Combust. Sci. Tech. Book Series.* **2**, ed. I. Glassman; Gordon and Breach, New York.

Law, C. K. (1995). Private communication.

Law, C. K. (1996). Private communication.

Lee, A., Jiang, Y. J., Zhu, D. L., and Law, C. K. (1992), "Burning-Rate Enhancement of Organic Diazide Propellants: Dihalide Addition and Pressure Elevation," *AIAA Journal*, Vol. 30, No. 5, pp. 1298–1303.

Lee, A., Law, C. K., and Makino, A. (1989), "Aerothermochemical Studies of Energetic Liquid Materials. 3. Approximate Determination of Some Thermophysical and Thermochemical Properties of Organic Azides," *Combustion and Flame*, Vol. 78, pp. 263–274.

Lee, A., Law, C. K., and Randolph, A. L. (1988), "Aerothermochemical Studies of Energetic Liquid Materials. 2. Combustion and Microexplosion of Droplets of Organic Azides," *Combustion and Flame*, Vol. 78, pp. 123–136.

Moriarty, R. M. and Rao, M. S. (1993), "Strained Hydrocarbons. Benzvalene and Derivatives." *Proceedings of the Sixth ONR Propulsion Meeting*, Boulder, CO, pp. 1–6.

Nielsen, L. E. (1978), *Predicting the Properties of Mixtures: Mixture Rules in Science and Engineering*, Marcel Dekker, Inc., New York.

Palopoli, S. F. and Brill, T. B. (1991), "Thermal Decomposition of Energetic Materials. 52. On the Foam Zone and Surface Chemistry of Rapidly Decomposing HMX," *Combustion and Flame*, Vol. 87, pp. 45–60.

Patankar, S. V. (1980), *Numerical Heat Transfer and Fluid Flow*, McGraw-Hill, New York.

Schiller, D., Bhatia, R., and Sirignano, W. A. (1996), "Energetic Fuel Droplet Gasification with Liquid-Phase Reaction," *Combust. Sci. Tech.*, Vols. 113–114, pp. 471–491.

Schiller, D., Li, J., and Sirignano, W. A. (1997), "Transient Heating, Gasification and Oxidation of an Energetic Liquid Fuel," submitted to *Combustion and Flame*.

Westbrook, C. K. and Dryer, F. L. (1981), "Simplified Reaction Mechanisms for the Oxidation of Hydrocarbon Fuels in Flames," *Combust. Sci. Tech.* Vol. 27, pp. 31–43.